Embolism resistance in petioles and leaflets of palms

Thaise Emilio, Laurent Lamarque, Jose Torres Ruiz, Andrew King, Guillaume Charrier, Régis Burlett, Maria Conejero, Paula J Rudall, William J Baker, Sylvain Delzon

Embolism resistance in petioles and leaflets of palms

Thaise Emilio[1,2,*], Laurent J. Lamarque[3], José M. Torres-Ruiz[4], Andrew King[5], Guillaume Charrier[4], Régis Burlett[3], Maria Conejero[1], Paula J. Rudall[1], William J. Baker[1] & Sylvain Delzon[3]

[1] Royal Botanic Gardens, Kew, Richmond, Surrey, TW9 3AB, UK, [2] Programa Nacional de Pós-Doutorado (PNPD), Programa de Pós Graduação em Ecologia, Institute of Biology, University of Campinas – UNICAMP. P.O. Box: 6109, Brazil, [3]BIOGECO, INRA, Université de Bordeaux, 33615 Pessac, France, [4]Université Clermont-Auvergne, INRA, PIAF, 63000, Clermont-Ferrand, France, [5]Synchrotron SOLEIL, L'Orme de Merisiers, 91190 Saint-Aubin – BP48, Gif-sur-Yvette Cedex, France

**For correspondence. Email thaise.emilio@gmail.com*

- **Background and aims** Hydraulic studies are currently biased towards conifers and dicotyledonous angiosperms; responses of arborescent monocots to increasing temperature and drought remain poorly known. This study aims to assess xylem resistance to drought-induced embolism in palms.
- **Methods** We quantified embolism resistance via P_{50} (xylem pressure inducing 50% of embolism or loss of hydraulic conductivity) in petioles or leaflets of six palm species differing in habitat and phylogenetic relatedness using three techniques: *in vivo* X-ray-based micro-computed tomography, *in situ* flow centrifuge and the optical vulnerability method.
- **Key results** Our results show that P_{50} of petioles varies greatly in the palm family from -2.2±0.4 MPa in *Dypsis baronii* to -5.8±0.3 MPa in *Rhapis excelsa* (Mean ± SE). No difference or weak differences were found between petioles and leaf blades within species. Surprisingly, where differences occurred, leaflets were less vulnerable to embolism than petioles. Embolism resistance in palms is not correlated with conduit size ($r = 0.37$, $p = 0.11$).
- **Conclusions** This study represents the first estimate of drought-induced xylem embolism in palms across biomes and provides the first step towards understanding hydraulic adaptations in long-lived arborescent monocots. It showed an almost three-fold range of embolism resistance between palm species, as large as that reported in all angiosperms. We found little evidence for hydraulic segmentation between leaflets and petioles in palms, suggesting that when it happens, hydraulic segregation may lack a clear relationship with organ cost or replaceability.

Key words: Arecaceae, palms, drought resistance, micro-CT x-ray, optical vulnerability method, P_{50}, synchrotron, xylem embolism resistance.

INTRODUCTION

Global warming is likely to result in a worldwide increase in aridity (Sherwood and Fu, 2014; Huang *et al.*, 2016). Dramatic changes in dry and wet periods are predicted for even the most humid regions (Duffy *et al.*, 2015). Therefore, it is critical to reliably predict the likelihood of a plant to succumb to drought. Interspecific patterns of drought-induced mortality are best predicted on a global scale by xylem resistance to embolism and particularly by the species' hydraulic safety margin (Anderegg *et al.*, 2016). Although data on xylem vulnerability have increased in recent decades, the available information is strongly biased towards conifers and dicotyledonous angiosperms (Choat *et al.*, 2012). In contrast, hydraulics of monocots remain poorly understood.

Monocots account for 25% of angiosperm species, including economically important plant families such as grasses, orchids, lilies and palms (Anderson and Janssen, 2009). Embolism resistance in monocots is known mostly for species in the grass family (e.g. Lens *et al.*, 2016) and more recently, bromeliads (Males, 2017). Embolism resistance in the palm family has been relatively poorly studied (though see Renninger and Phillips, 2011). Palms are important components for carbon (Fauset *et al.*, 2015) and water cycling (Renninger and Phillips, 2010a) in tropical forests. Yet the role of palms as ecosystem engineers and their potential decline under climate change have been neglected due to a relative lack of understanding of their hydraulic functioning.

The palm family (Arecaceae) includes more than 2,600 species and 181 genera distributed in tropical and subtropical regions worldwide (Baker and Dransfield, 2016). Over 90% of palm species are restricted to tropical rainforests (Couvreur *et al.*, 2011), though intriguingly, large arborescent palms can also occur in extremely arid climates such as deserts. Palms differ strongly, both morphologically and functionally, from other species in

their respective ecosystems, including the large woody trees (dicotyledonous and coniferous) that dominate forests worldwide and the small herbaceous grasses that dominate open environments (Tomlinson, 2006). Most of the factors that make palms hydraulically distinct are potentially linked to three key features. First, palms are perennial long-lived plants lacking dormancy mechanisms to avoid seasonally unfavourable environmental conditions. Second, palms (like all monocots) lack a vascular cambium and both xylem and phloem cells need to remain functional throughout an individual lifespan. Third, the early loss of the primary root that characterizes all monocots (which in dicotyledonous trees develops into a branching tap root) restricts access to deep soil water. These differences – sometimes expressed as constraints (e.g. Alves *et al.*, 2004; Tomlinson, 2006) – are linked to the dominance in monocots of herbaceous life-forms other than trees.

The lack of a vascular cambium in monocots restricts thickening growth and may result in reduced efficiency for secure water transport when achieving greater stature. Many monocots combine a vessel-based root xylem system with an entirely tracheid-based xylem system in the stem and leaf (Carlquist, 2012). The relative lack of vessels in aerial parts makes monocots more efficient in avoiding the spread of air embolism, but also restricts plant size, water flow and transpiration (Carlquist, 2012). However, palms appear to have overcome this limitation by displaying a broad range of size and growth forms, almost equivalent to that of all other tropical plant groups combined (Couvreur *et al.*, 2015). Even though they lack 'true' secondary growth by means of a vascular cambium, different palm species can achieve heights as tall as eudicot trees and develop climbing stems that exceed the length of any vascular plant (Tomlinson, 2006). Like dicot trees, arborescent palms taper their vessels from the base to the apex of the plant to overcome hydrodynamic resistance to water flow from root to leaf (Petit *et al.*, 2014). The tallest palm (*Ceroxylon quindiuense*) can grow up to 61 metres in height (Bernal *et al.*, 2018) and there is no evidence for hydraulic

limitation in height for large canopy palms living under non-limiting water conditions (Renninger and Phillips, 2011).

The hydraulic efficiency of the vascular architecture of palms surpasses the theoretical hydraulic conductivity of all tropical and temperate trees (Renninger *et al.*, 2013). This is because palms, as monocots in general, have broader vessels than dicots (Olson *et al.*, 2014). In contrast with other monocots, many palms have broad vessels distributed along all vegetative organs (Carlquist, 2012). Broader vessels make palms efficient in water transport, but this strategy can have its drawbacks. Embolism resistance can decrease with increase in vessel diameter (Hacke *et al.*, 2006), which suggests that palm xylem would potentially be vulnerable to embolism (Carlquist, 2012). Although the trade-off between xylem efficiency and safety is weaker than previously thought, conduit diameter still imposes an upper limit for hydraulic safety (Gleason *et al.*, 2016).

Structurally, xylem safeguarding in palms can be achieved by discontinuity between stem and leaf vessels (Tyree and Zimmermann, 2002). Leaf-trace linkage to the stem xylem occurs entirely via protoxylem elements (Tomlinson, 1990), which in palms are mainly tracheids rather than vessels (Tomlinson *et al.*, 2011). The protoxylem and metaxylem connection occurs deep within the central stem cylinder (Tomlinson, 1990), securing a long distance between transpiring leaves, where embolism is more likely, and the axial xylem system, where embolism must be avoided at all costs. Even within the same vascular bundle, vessels in palms may not share intercellular pathways but can be separated by several layers of parenchymatous cells, potentially representing an adaptation for preventing embolism spread between vessels (Tyree and Zimmerman, 2002). Extreme examples of xylem segmentation between leaf and stem xylem is observed in climbing rattan palms of the genus *Calamus*, in which there is no connection between protoxylem and metaxylem even within the same bundle (Tomlinson *et al.*, 2001).

It was early hypothesized that palms restrict embolism to their expendable leaves to prevent embolism generating irreversible damage to their long-lived stems and to assure continued growth of the plant (Zimmermann, 1982; Zimmermann and Sperry, 1983; Sperry, 1985). However, it is unlikely that palm species rely exclusively on hydraulic segmentation for the maintenance of their hydraulic functioning. Palms store large amounts of water in their trunks and nearly 20% of their daily transpiration can be sustained by this source (Sperling *et al.*, 2015, Renninger *et al.*, 2009, Renninger and Phillips, 2010b). This effect is negligible in some dicotyledonous and coniferous trees with relatively small amounts of parenchyma (Jupa *et al.*, 2016), but it can be significant in plants such as palms, in which parenchyma can occupy more than 50% of the cross-sectional area (Renninger and Phillips, 2010b).

Embolism resistance describes the lethal threshold of dehydration in plants beyond which the plant fails to recover (Urli *et al.*, 2013). Thus, embolism resistance sets the upper limit of plant transpiration, with impacts for photosynthesis productivity (Brodribb, 2009) and ultimately biome colonization (Choat *et al.*, 2012). Palms have wider vessels, smaller amounts of vessel-to-vessel connections and higher proportions of parenchymatous tissue than other plants for which hydraulic data are available. All these features are expected to affect drought resistance, but the extent to which they render palms more or less vulnerable than other plants is unknown.

Palms rely on early-formed xylem vessels for their entire life, which can in some cases exceed a hundred years (Tomlinson, 2006). Limited evidence has shown that some palms are resistant to embolism onset (Sperry, 1985; Renninger and Phillips, 2011), but the scarce data on palm hydraulics are insufficient to identify the range of variation in embolism resistance. In this paper, we determine the embolism resistance of six palm species from different biomes and compare them with the broad range of embolism resistance previously

reported in angiosperms and conifers. To test the hydraulic segmentation hypothesis, we monitor embolism formation and spread in palm leaves with different amounts of parenchyma and compare leaf and petiole P50 values.

MATERIAL AND METHODS

Plant material

We selected twelve palm species for the experiments (Supplementary data Table S1), mostly belonging to the two most widely cultivated palm subfamilies Arecoideae and Coryphoideae. We targeted species that show a wide range of natural habitats (Supplementary data Fig. S2). Plants of *Chamaedorea radicalis* Mart., *Howea forsteriana* (F.Muell.) Becc, *Rhapis excelsa* (Thunb.) A.Henry and *Trachycarpus fortunei* (Hook.) H.Wendl. were used for direct micro-CT visualization of embolism formation. Plants from 0.6 to 1.2 m in height, depending on species, were sourced from a commercial nursery (A L'Ombre des Figuiers, Pluguffan, France). A second set of plants was used for experiments at the UMR-BIOGECO laboratory (University of Bordeaux, France). Additionally, for the experiments at UMR-BIOGECO, excized leaf petioles from adult plants of *Calamus longipinna* K.Schum. & Lauterb., *Chamaedorea seifrizii* Burret, *Dypsis baronii* (Becc.) Beentje & J.Dransf., *Dypsis decaryi* (Jum.) Beentje & J.Dransf. and *Dypsis lutescens* (H.Wendl.) Beentje & J.Dransf., *Phoenix canariensis* Chabaud, *Rhapis subtilis* Becc., *Salacca ramosiana* Mogea, were sourced from RBG Kew living collections (Richmond, United Kingdom).

Embolism visualization in intact plants (micro-CT)

A first set of twelve plants was shipped to the SOLEIL synchrotron (Paris, France) in April 2017 for direct micro-CT visualization of embolism formation two days before the dehydration experiments started. The first scan was performed on the petiole of well-watered

plants while they were still potted to quantify the presence of any native embolism events. After the first scan, plants were removed from the pots and the soil carefully removed from the roots. Uprooted plants were allowed to dry on the bench for the duration of the experiments (3 to 6 days). For each scan, the intact plant was placed in the rotating stage and their petioles were fixed to minimize the risk of movements during the tomography.

Observations were conducted at the SOLEIL microCT PSICHÉ beamline (King *et al.*, 2016). The petioles of three 1.5-m tall intact palms were scanned using a high flux (3.1011 photons mm $^{-2}$), 25 keV monochromatic X-ray beam, while being rotated from 0° to 180° using a continuous rotation mode. Thanks to the high load capacity and free central aperture of the rotation stage, imaging cross sections were also selected near the middle of the petiole. Dehydration was progressively induced in the three bare-rooted plants per species by stopping irrigation and exposing them to a fan to accelerate the process. X-ray projections were collected with a 50-ms exposure time during rotation and recorded with an Orca-flash sCMOS camera (Hamamatsu Photonics K.K., Naka-ku, Japan) equipped with a 250-µm thick LuAG scintillator. The scan time was 120 s for each sample and yielded a stack of 2048 TIFF image slices. Each petiole was scanned once throughout the dehydration of each individual and up to 11 petioles were scanned per species. Tomographic reconstructions were conducted using the Paganin method (Paganin *et al.*, 2002) in PyHST2 software (Mirone *et al.*, 2014) and resulted in 2-bit volumic images with a 3.02 µm voxel resolution.

The water potential of the plant was measured from a detached leaf with a Scholander-type pressure chamber (DG Meca, Gradignan, France) immediately after each scan. The plant was then allowed to dry until the next scan. The scans were spaced 6–24 hours apart, depending on the species and dehydration stage. A maximum of four scans were taken per plant and we did not observe any evidence of damage during the experiments. The experiment ended when the plant embolism percentage was near 100%. Subsequently, an

additional scan was performed after removing the segment immediately above the scanned area (*ca* 1 mm) to embolize all the vessels artifactually. This final cut scan was then used as reference scan to estimate the maximum area of embolized vessels.

The areas of embolized and functional vessels were determined in each scan image using Image J software (NIH). Conduit diameter (D) for each vessel was calculated as following:

$$D = 2 \times \sqrt{(A/\pi)} \quad \text{(Eq.1)}$$

where A is the area of the vessel. The sum of conduit diameter from the reference scans was used to calculate the maximum theoretical conductivity and from the scans taken during the bench dry experiment used to calculate the theoretical conductivity at each water potential according to the Hagen–Poiseuille equation:

$$K_{th} = \Sigma \pi D^4/128\ \eta \quad \text{(Eq.2)}$$

where D is the vessel diameter and η is the viscosity of water (1.002 MPa s^{-1} at 20 $^{\circ}C$). The percentage loss of xylem conductance (PLC) for each scan was then calculated from the conductivity of the functional vessels observed in each scan as a function of the maximum theoretical conductivity:

$$PLC = 100 \times (1 - K_{psi}/K_{max}) \quad \text{(Eq. 3)}$$

where K_{psi} is the theoretical conductivity of the functional vessels and K_{max} is the maximum theoretical conductivity.

Embolism visualization in detached leaves (OV technique)

The onset and accumulation of embolism during palm leaf desiccation were monitored on five to six individuals per species using the optical vulnerability method (hereafter OV technique, Brodribb *et al.*, 2016; full details available at

http://www.opensourceov.org). Briefly, all individuals were kept well hydrated prior to measurements. During the experimental set-up, where palms had to be uprooted, both roots and non-scanned leaves were kept bagged to avoid water loss by transpiration. Only after complete installation of the scanner and psychrometer, the targeted leaf was excized from the plant at least 30 cm from the scan location. The first embolism event was observed at least 12 hours after excision, confirming that no detectable embolism was caused by leaf excision.

For each individual, two leaflets were placed on a scanner (Perfection V800 Photo, EPSON, Suwa, Japan) and fixed with a transparent glass and adhesive tape to minimize leaf movement during dehydration. Scan magnification, brightness and contrast as well as leaf area were set to optimize visualization of embolisms in both main and cross veins. Each leaflet was automatically scanned every five minutes using a computer automation software (AutoIt 3) until mesophyll cells turned brown, indicating cell death.

Water potentials were recorded every 30 min using a stem psychrometer (ICT International, Armidale, NSW, Australia) that was attached to the petiole a few centimetres below the scanned leaflets. Accuracy of the readings was double-checked by periodically measuring xylem water potentials on neighbouring leaflets using a Scholander pressure chamber (DG Meca, Gradignan, France). Once completed, stacks of images were analyzed using ImageJ (National Institute of Health, New York, NY, USA) to highlight embolism events that occurred throughout dehydration (for the detailed procedure, see Brodribb *et al.*, 2016 and the website https://github.com/OpenSourceOV/image-processing-instructions). The cumulative percentage embolized area dataset obtained was then coupled with the corresponding water potential sequences. Vulnerability curves were constructed as percentage embolism function of water potential.

Hydraulic measurements of embolism resistance (Cavitron)

Resistance to drought-induced embolism in the petioles was determined using *in-situ* flow centrifuge technique (Cavitron, Cochard *et al.*, 2005) at the GENOBOIS hydraulic platform.

As techniques that build vulnerability curves from plant sections can suffer from open-vessel artefact (see Torres-Ruiz, 2017, Cochard *et al.*, 2013), three samples per species were used to test for open-vessel artefact (Torres-Ruiz *et al.*, 2017) by injecting air at 2 bars at one end. Eight species failed the open-vessel artefact test, produced unsatisfactory vulnerability curves and were removed from our analysis. Unfortunately, we were unable to obtain cavitron data for any of the species for which we collected data using microCT and OV techniques, limiting cross-validation among all techniques.

No open-vessel artefact was detected for four palm species: *D. baronii*, *D. decaryi*, *D. lutescens*, *T. fortunei*. For those species, petioles were recut under water with a razor blade to a standard length of 0.27 m and infiltrated with a reference ionic solution of 10 mm 25 KCl and 1 mm $CaCl_2$ in deionized ultrapure water. Centrifugal force was used to generate negative pressure into the xylem and induce embolism with a rotor of 0.27 m diameter. This method allows measurement of xylem conductance under negative pressure using the custom software Cavisoft 4.0 (Univ. Bordeaux, Pessac, France). Initially, the maximum conductance of petioles (in $m^2MPa^{-1}s^{-1}$) was calculated under low xylem pressures. The percentage loss of xylem conductance of the petioles was calculated at different xylem pressures from -0.8 to -9 MPa with Eq 3, except for *T. fortunei*, where only a negligible loss of conductance was measured even in the most negative water potentials.

Vulnerability curves

Embolism resistance in plants is commonly expressed by the xylem pressure inducing 50 percent loss of conductivity or its equivalent in embolized area (P_{50}: Choat *et al.*, 2012).

This embolism resistance parameter can be calculated from xylem vulnerability curves, a two-dimensional graph relating percentage of xylem conductance loss and xylem pressure (Cochard *et al.*, 2013). Vulnerability curves were obtained with the three different techniques (micro-CT, OV and Cavitron). For each sample, the relationship between percentage of xylem conductance loss/percentage of embolized pixels and xylem water pressure was fitted with the following sigmoidal equation (Pammenter and Vander Willigen, 1998):

$$PLC = 100 / (1 + \exp (S/25*(P_i - P_{50}))) \quad \text{(Eq. 4)}$$

where P_{50} (MPa) is the xylem pressure inducing a 50% loss of conductivity and S (% MPa-1) is the slope of the vulnerability curve at the inflection point.

Statistical analysis

Individual vulnerability curves were obtained per sample from OV and cavitron. To calculate the value of embolism resistance per species, the values of P_{50} of all the samples were averaged. A single vulnerability curve was obtained based on the micro-CT method. In this case, the value of embolism resistance per species is given by the P_{50} of the single curve adjusted from multiple individual data points. Embolism resistance differences between petiole and leaflets was tested using one-sample t-test, since only a single vulnerability curve was obtained for petioles in most cases. We compared embolism resistance in petioles by analysis of variance followed by Tukey's multiple comparisons with 95% family-wise confidence level. Pearson's linear correlations were performed to test for correlations between embolisms resistance and conduit size.

Vulnerability curve fitting with the NLIN procedure in SAS 9.4 (SAS Institute Inc., Cary, NC, USA). Three-dimensional reconstructions visualizations of plant petioles were generated with Drishti volume exploration and presentation tool (Limaye, 2012). All remaining data manipulation, analysis and plots were performed in R v.3.5.1 (R Core Development Team, 2018) unless otherwise stated.

RESULTS

Embolism resistance in palm leaves and petioles

Embolism resistance was characterized in the petioles of six palm species that differed in habitat and phylogenetic relatedness (Supplementary data Table S1) using three different techniques: *in vivo* X-ray based micro-computed tomography, *in situ* flow centrifuge and the optical vulnerability method. We found a large and significant variation in P_{50} between species ($F = 71.3$, $p<0.01$, Table 1), ranging from -2.24 ± 0.4 MPa in *D. baronii* to -5.82 ± 0.3 MPa in *R. excelsa* (Mean ± SE). Embolism resistance in *R. excelsa* differed significantly from all other species (Table 1). Moreover, palm petioles showed an embolism resistance range equivalent to that observed for angiosperms across all the biomes in which palms grow naturally (Fig.1).

No difference or weak differences in P_{50} were observed between petiole and leaflet across the three studied species (Fig.2). The difference was significant only in *C. radicalis* ($t = -3.463$, $p = 0.013$), showing leaflets more resistant than petioles, but not in *R. excelsa* ($t = -0.121$, $p = 0.909$) or *H. forsteriana* ($t = -2.456$, $p = 0.068$). Embolism resistance in petioles is not correlated with conduit size across species (Pearson' correlation $r = 0.37$, $p = 011$, Supplementary data Fig. S3). Larger vessels embolized first in *R. excelsa*, whereas not at all in *C. radicalis* and *H. forsteriana* (Fig.3, Supplementary data Table S4).

Micro-CT observation of embolism formation in palm petioles

High-resolution micro-CT images allowed visualization of vessel embolism in petioles of intact plants (Fig. 4). We observed the first embolism events within 1 to 3 days after the start of the bench dry experiments. After onset of embolism, the embolism spreads towards most of vessels following small changes in water potential. The first embolism events were observed below -2 MPa in *C. radicalis*, -2.2 MPa in *H. forsteriana*, -5.3 MPa in *R. excelsa* and -5.8 MPa in *T. fortunei*. Within six to 24 hours after the first events, most of the vessels were embolized in all species except *T. fortunei*. The largest amount of embolism observed for *T. fortunei* with micro-CT was *ca* 4% at -8 MPa (Supplementary data Fig. S5) and no vulnerability curve was obtained for this highly resistant species.

In well-hydrated plants, water is stored not only in parenchyma cells but also in intercellular spaces. We observed high amounts of water in intercellular spaces in *C. radicalis* and *H. forsteriana*, and smaller amounts in *R. excelsa* and *T. fortunei* (Fig. 5). A high proportion of hydrated petiole tissue consists of parenchyma (85% in *C. radicalis*, 75% in *H. forsteriana*, 74% in *R. excelsa* for the samples shown in Fig. 4). When leaves dry out, parenchyma tissue contracts and petioles shrink. Petiole shrinkage displays remarkable differences between species (*cf.* Fig. 4). We observed a reduction in petiole cross-sectional area of 14% in *C. radicalis*, 40% in *H. forsteriana* and 60% in *R. excelsa* at advanced stages of embolism when most of the vessels were embolized. Xylem embolism resistance between species coincides with trends of shrinkage rather than tissue proportion. Expansion of air space within the *C. radicalis* petiole reduced area shrinkage for this species.

Optical visualization of embolism spread in palm leaflets

Embolism spread in the leaflet was visualized using the OV technique (Fig. 6). We observed the first embolism within 12 hours (-4.0 Mpa in *R. excelsa*) to 30 days (-3.41 MPa

in *C. radicalis*) after the start of the experiments. Within 1 (-10.11 MPa in *R. excelsa*) to 18 days (-3.66 MPa in *C. radicalis*) after the first events, all vessels were embolized. The time to embolism spread can be ten-fold in palms (Supplementary data Fig. S6, left). In our experimental design, *C. radicalis* took from twenty to forty days to dehydrate, compared with less than four days in *R. excelsa.* Large parallel veins were the first to be embolized (Fig 4a, d, g). Subsequently, embolism spread to the secondary minor parallel and cross-veins.

We observed leaflet shrinkage during the bench-dry experiments using the OV method for all samples. Most of the shrinkage in palm leaflets occurs longitudinally as a result of the parallel disposition of the major veins. Within species, longitudinal shrinkage varies from 3–8% to almost 40% (Supplementary data Table S7). Interestingly, most leaflet shrinkage occurred after embolism onset in all three palm species (Supplementary data Movie S8, S9, S10,). This shrinkage was most evident in *C. radicalis* (Supplementary data Movie S8, where it was possible to observe embolism spread (as change in reflectance inside the main vessels), tracking the advance of the dehydration front from the left (tip) to right (base) of the leaflet.

DISCUSSION

Broad range of embolism resistance in palms

This study provides the first estimate of drought-induced xylem embolism resistance in palms originating from a range of different biomes. Our results add novel information to previous studies demonstrating that palms encompass a relatively broad range of embolism resistance - from low in *Dypsis baronii* to high in *Rhapis excelsa*. To our knowledge, embolism resistance has previously been investigated in only four palm species (Sperry, 1985; Cobb, 2006; Renninger and Phillips, 2011). Sperry (1985) found that in *R. excelsa* embolism

induction commences when xylem pressure falls below *ca* -3 MPa. Similarly, our study of *R. excelsa* found no embolism at relatively high water potentials in both leaves and petioles. At the opposite end of the spectrum, Renninger and Phillips (2011) found low resistance to embolism in the Amazonian species *Iriartea deltoidea* (P_{50} = -1.4 MPa). All the palms in our study were more resistant to embolism than *I. deltoidea*, demonstrating that palms can be as resistant as other angiosperm species, including both herbs and trees.

Embolism resistance and monocot hydraulic architecture

The mechanisms by which palms achieve such a wide range of embolism resistance remain unclear and merit further investigation. The hydraulic-segmentation hypothesis predicts that vulnerability to embolism will be relatively high in plant parts that are more expendable (Tyree & Zimmerman 2002). However, we found little evidence for segmentation between leaflet and petioles in palms. This result is consistent with the fact that palms do not drop leaflets under drought stress. Instead, leaflets tend to dry out from the tip to the base (c.f. Fig. 3 a to c). These observations are in agreement with the results of previous studies that show little difference in embolism resistance between organs of an herbaceous plant (Skelton *et al.* 2017), though in woody angiosperms hydraulic segmentation seems to be species-specific (Dominguez-Rodriguez *et al.* 2018, Klepsch *et al.*, 2018, Losso *et al.*, 2018). Surprisingly, we observed leaflets being less vulnerable to embolism than petioles in the sole species – *C. radicalis* - where we observed significant differences between proximal and distal parts of the leaf. This result offers novel evidence showing that hydraulic segregation can occur without a clear relationship with organ cost or replaceability.

Pit membrane thickness, an important predictor of embolism resistance in woody plants (Lens *et al.*, 2013; Li *et al.*, 2013), is also unlikely to play a major role in palm embolism resistance. Most palms possess only one to few metaxylem vessels per vascular

bundle in transverse section (Thomas and Boura, 2015). Therefore, connections between metaxylem vessels (and therefore, embolism spread) occur via transversal commissures (Tomlinson, 1990). Those transversal commissures are smaller in diameter than metaxylem vessels and may contribute to embolism resistance. Our microCT observations on the most resistant species, *T. fortunei*, support this hypothesis. For this species, we observed that two vessels can be connected through one of these commissures without spread of embolism from the embolized to the functional vessel (Supplementary data Fig. S11).

The relatively unusual co-occurrence of tracheids and vessels in palms has also been suggested as a strategy to cope with drought, as found in another monocot, the Australian resurrection plant *Borya*, in which vessel elements can offer a rapid supply of water in the rainy season, while thick-walled tracheids maintain the water column under higher tension during the dry season (Carlquist, 2012). However, our data do not offer support to this hypothesis, as we did not observe functional tracheids in the presence of embolized metaxylem vessels.

Embolism resistance describes the lethal threshold of dehydration beyond which the plant fails to recover (Urli *et al.*, 2013). Many other hydraulic traits (e.g. rooting depth, transpiration rate, and tissue capacitance) will dictate how fast a plant approaches this threshold (Brodribb, 2017). For the first time in intact palms, we imaged leaf petiole parenchyma shrinkage and tissue collapse while the leaf water potential decreases (cf. Fig. 1). Changes in size and shape of palm petioles are noticeably higher than those observed in other species studied previously using the same methods (e.g. Cochard *et al.*, 2015; Nolf *et al.*, 2017). Significative amounts of petiole shrinkage occur even before the plant reaches a water potential that induces lethal embolism. The proportion of parenchyma that we observed in palm petioles compares closely with that observed in succulent plants (Morris *et al.*, 2016). Together, these observations indicate that water storage in palm petioles (as well as in stems)

could play an important role in preventing embolism while maintaining a high transpiration rate.

Petiole capacitance in palms extends the threshold of drought tolerance conferred solely by xylem structural features, rendering palm xylem more resistant than was previously predicted based on their large vessels. This mechanism was already described for tropical tree species with high capacitance that can avoid embolism by releasing stored water from parenchyma to the xylem (Meinzer *et al.*, 2008). The role of water storage in drought tolerance and mortality may be especially important when the drought results from increasing seasonality rather than merely decreasing rainfall. The ability to store water that can sustain transpiration until water again becomes available could ultimately be as important in changing climates as embolism resistance.

Challenges and perspectives in estimating embolism resistance in palms

One of the palm species in this study, *T. fortunei*, appeared to be so resistant to embolism that even achieving the water potential where the plant has lost 50% of function was challenging. Even in less extreme cases, estimating embolism resistance in palms is difficult. Cobb (2006) measured embolism resistance for the climbing palm *Calamus caryotoides* using the single-vessel air-seeding technique, but concluded from the low mean air-seeding pressure and wide variation that this technique is unsatisfactory for species with monocot anatomy where vessels occur in isolation. Renninger and Phillips (2011) used both an air-pressure method (*Washingtonia robusta*) and a bench-dry method (*Iriartea deltoidea*) to hydraulically measure changes in the xylem conductivity of palms. However, the exponential shape of their vulnerability curves for *Washingtonia robusta* should be interpreted with caution, as it has recently been shown that this shape is most likely to result from an open-vessel artefact (Torres-Ruiz *et al.*, 2014).

The weak differences in embolism resistance between leaflets and petiole found in our study indicate that in palm species, P_{50} can be characterized from either leaf petioles or leaflets. In this sense, the novel non-invasive optical method (Brodribb *et al.*, 2016) appears particularly promising for phenotyping palm drought-induced embolism resistance.

CONCLUSIONS

Knowledge of drought resistance strategies in a plant group that is as ecologically and economically important as palms represents a significant step towards understanding how plants respond to drought in both natural and agricultural systems. This study provides the first estimate of drought-induced xylem embolism in palms across biomes. Although the mechanisms by which palms achieve embolism resistance in their wide vessels are not entirely clear, it is likely that they protect their large xylem vessels from embolism by mobilizing water from parenchyma tissues to the vessels, thus preventing achievement of embolism-inducing tensions. This investigation provides the first step towards understanding hydraulic adaptations in palms by showing how high embolism resistance can be sustained in long-lived arborescent monocots. Further investigations of mechanisms of embolism resistance across palm lineages should improve our understanding of both species distribution and their susceptibility to drought that underpins the role of palms in tropical ecosystems.

SUPPLEMENTARY DATA

Supplementary data are available online at https://academic.oup.com/aob and consist of the following. Table S1: species studied, their distribution and habitat. Figure S2: Palm species occurrence optimum along the gradients of water-table depth and aridity. Figure S3: Relationship between xylem pressure and the mean area of embolized conduits. Table S4: Observed and estimated vessel mean per micro-CT scan, species and xylem water potential.

Figure S5: Two-dimensional (2D) digital cross-section X-ray microtomography (micro-CT) of *Trachycarpus fortunei*. Figure S6: Accumulation of embolisms over time for three palm species (*Chamaredorea radicalis, Howea, forsteriana* and *Rhapis excelsa*). Table S7: leaflet shrinkage percentages per sample. Movies S8–S10: examples of leaf dehydration and shrinkage. Figure S11: transverse section of *Trachycarpus fortunei*. Movie S12. Time comparison of embolism propagation between species.

FUNDING

This work was supported by European Union's Horizon 2020 research and innovation programme under the Marie Sklodowska-Curie grant agreement No 706011 (PalmHydraulics); SOLEIL synchrotron facility, PSICHE beamline (grant number: 20160990); the program "Investments for the Future" (grant number ANR-10-EQPX-16, XYLOFOREST) from the French National Agency for Research; IdEx Bordeaux International Post-doctoral Program (grant number UB101 CR1024-R s/CR1024-6M to L. J. L.) and by the Coordenação de Aperfeiçoamento de Pessoal de Nível Superior - Brasil (CAPES) –Finance Code 001.

ACKNOWLEDGEMENTS

We thank the We thank Scott Taylor, David Cook, Silke Roch and Wanyi Zuo for their help on sampling living collections and Chrissie Prychid for her help in the imaging labs at the Royal Botanic Gardens, Kew and Ruth Phoebe TchanaWandji for her help with the cavitron and micro-ct image analysis at UMR-BIOGECO, Amy Zanne for her help with Synchrotron data collection.

LITERATURE CITED

Alves LF, Martins FR, Santos FAM. **2004**. Allometry of a neotropical palm, *Euterpe edulis* Mart. *Acta Botanica Brasilica* **18**: 369–374.

Anderegg WRL, Klein T, Bartlett M, Sack L, Pellegrini AFA, Choat B, Jansen S. **2016**. Meta-analysis reveals that hydraulic traits explain cross-species patterns of drought-induced tree mortality across the globe. *Proceedings of the National Academy of Sciences* **113**: 5024–5029.

Anderson CL, Janssen T. **2009**. Monocots. In: Hedges SB, Kumar S, eds. Timetree of life. New York: Oxford University Press, 203–212.

Baker WJ, Dransfield J. **2016**. Beyond Genera Palmarum: progress and prospects in palm systematics. *Botanical Journal of the Linnean Society* **182**: 207–233.

Bernal R, Martínez B, Sanín MJ. **2018**. The world 's tallest palms. *Palms* **62**: 5–16.

Brodribb TJ. **2017**. Progressing from 'functional' to mechanistic traits. *New Phytologist* **215**: 9–11.

Brodribb TJ, Bienaimé D, Marmottant P. **2016**. Revealing catastrophic failure of leaf networks under stress. *Proceedings of the National Academy of Sciences of the United States of America* **113**: 4865–4869.

Brodribb TJ. 2009. Xylem hydraulic physiology: the functional backbone of terrestrial plant productivity. *Plant Science* **177:** 245-251.

Carlquist S. **2012**. Monocot Xylem Revisited: New Information, New Paradigms. *The Botanical Review* **78**: 87–153.

Choat B, Jansen S, Brodribb TJ, Cochard H, Delzon S, Bhaskar R, Bucci SJ, Feild TS,

Gleason SM, Hacke UG, *et al.* 2012. Global convergence in the vulnerability of forests to drought. *Nature* **491**: 752–755.

Cobb AR. **2006**. Water relations in rattans.

Cochard H, Delzon S, Badel E. 2015. X-ray microtomography (micro-CT): a reference technology for high-resolution quantification of xylem embolism in trees. *Plant, Cell & Environment* **38**:201-206.

Cochard H, Badel E, Herbette S, Delzon S, Choat B, Jansen S. **2013**. Methods for measuring plant vulnerability to cavitation: A critical review. *Journal of Experimental Botany* **64**: 4779–4791.

Cochard H, Damour G, Bodet C, Tharwat I, Poirier M, Améglio T. **2005**. Evaluation of a new centrifuge technique for rapid generation of xylem vulnerability curves. *Physiologia Plantarum* **124**: 410–418.

Couvreur TLP, Forest F, Baker WJ. **2011**. Origin and global diversification patterns of tropical rain forests: Inferences from a complete genus-level phylogeny of palms. *BMC Biology* **9**: 44.

Couvreur TLP, Kissling WD, Condamine FL, Svenning JC, Rowe NP, Baker WJ. **2015**. Global diversification o f a tropical plant growth form: Environmental correlates and historical contingencies in climbing palms. *Frontiers in Genetics* **5**: 1–18.

Duffy PB, Brando P, Asner GP, Field CB. **2015**. Projections of future meteorological drought and wet periods in the Amazon. *Proceedings of the National Academy of Sciences of the United States of America* **112**: 13172–13177.

Fauset S, Johnson MO, Gloor M, Baker TR, Monteagudo M A, Brienen RJW, Feldpausch TR, Lopez-Gonzalez G, Malhi Y, ter Steege H, *et al.* 2015. Hyperdominance

in Amazonian forest carbon cycling. *Nature communications* **6**: 6857.

Gleason SM, Westoby M, Jansen S, Choat B, Hacke UG, Pratt RB, Bhaskar R, Brodribb TJ, Bucci SJ, Cao K, *et al.* 2016. Weak tradeoff between xylem safety and xylem-specific hydraulic efficiency across the world's woody plant species. *New Phytologist* **209**: 123–136.

Hacke UG, Sperry JS, Wheeler JK, Castro L. 2006. Scaling of angiosperm xylem structure with safety and efficiency. *Tree physiology* **26**: 689–701.

Huang J, Yu H, Guan X, Wang G, Guo R. 2016. Accelerated dryland expansion under climate change. *Nature Climate Change* **6**: 166–171.

Jupa R, Plavcová L, Gloser V, & Jansen S. 2016. Linking xylem water storage with anatomical parameters in five temperate tree species. *Tree physiology* **36**: 756-769.**King A, Guignot N, Zerbino P, Boulard E, Desjardins K, Bordessoule M, Leclerq N, Le S, Renaud G, Cerato M, *et al.* 2016**. Tomography and imaging at the PSICHE beam line of the SOLEIL synchrotron. *Review of Scientific Instruments* **87**: 093704.

Klepsch M, Zhang Y, Kotowska MM, Lamarque LJ, Nolf M, Schuldt B, Torres-Ruiz JM, Qin D-W, Choat B, Delzon S, *et al.* 2018. Is xylem of angiosperm leaves less resistant to embolism than branches? Insights from microCT, hydraulics, and anatomy. *Journal of Experimental Botany* **69**: 5611–5623.

Limaye A. 2012. Drishti: a volume exploration and presentation tool. *In Developments in X-ray Tomography VIII (Vol. 8506, p. 85060X).* International Society for Optics and Photonics.**Lens F, Picon-Cochard C, Delmas C EL, Signarbieux C, Buttler A, Cochard H, Jansen S, Chauvin T, Chacon Doria L, del Arco M, *et al.* 2016**. Herbaceous angiosperms are not more vulnerable to drought-induced embolism than angiosperm trees. *Plant Physiology* **172**: 661–677.

Lens F, Tixier A, Cochard H, Sperry JS, Jansen S, Herbette S. **2013**. Embolism resistance as a key mechanism to understand adaptive plant strategies. *Current Opinion in Plant Biology* **16**: 287–292.

Li S, Lens F, Espino S, Karimi Z, Klepsch M, Schenk HJ, Schmitt M, Schuldt B, Jansen S. **2016**. Intervessel pit membrane thickness as a key determinant of embolism resistance in angiosperm xylem. *IAWA Journal* **37**: 152–171.

Losso A, Bär A, Dämon B, Dullin C, Ganthaler A, Petruzzellis F, Savi T, Tromba G, Nardini A, Mayr S and Beikircher B. 2019. Insights from in vivo micro-CT analysis: testing the hydraulic vulnerability segmentation in Acer pseudoplatanus and Fagus sylvatica seedlings. *New Phytologist* **221**: 1831-1842.

Males J. **2017**. Hydraulics link leaf shape and environmental niche in terrestrial bromeliads. *Biotropica* **49**: 891–902.

Meinzer FC, Woodruff DR, Domec J-C, Goldstein G, Campanello PI, Gatti MG, Villalobos-vega R. **2008**. Coordination of leaf and stem water transport properties in tropical forest trees. *Oecologia* **156**: 31–41.

Mirone A, Brun E, Gouillart E, Tafforeau P, Kieffer J. **2014**. The PyHST2 hybrid distributed code for high speed tomographic reconstruction with iterative reconstruction and a priori knowledge capabilities. *Nuclear Instruments and Methods in Physics Research Section B: Beam Interactions with Materials and Atoms* **324**: 41–48.

Morris H, Plavcová L, Cvecko P, Fichtler E, Gillingham MAF, Martínez-Cabrera HI, Jansen S, Wheeler E, Zheng J, Ziemińska K, *et al.* 2016. A global analysis of parenchyma tissue fractions in secondary xylem of seed plants. *New Phytologist* **209**: 1553–1565.

Nolf M, Lopez R, Peters JM, Flavel RJ, Koloadin LS, Young IM, Choat B. 2017.

Visualization of xylem embolism by X-ray microtomography: a direct test against hydraulic measurements. *New Phytologist* **214:**890-898.

Olson ME, Anfodillo T, Rosell J a., Petit G, Crivellaro A, Isnard S, León-Gómez C, Alvarado-Cárdenas LO, Castorena M. **2014**. Universal hydraulics of the flowering plants: Vessel diameter scales with stem length across angiosperm lineages, habits and climates. *Ecology Letters* **17**: 988–997.

Paganin D, Mayo SC, Gureyev TE, Miller PR, Wilkins SW. **2002**. Simultaneous phase and amplitude extraction from a single defocused image of a homogeneous object. *Journal of Microscopy* **206**: 33–40.

Pammenter NW, Vander Willigen C. **1998**. A mathematical and statistical analysis of the curves illustration vulnerability of xylem to cavitation. *Tree Physiology* **18**: 589–593.

Petit G, DeClerck FAJ, Carrer M, Anfodillo T, Phillips N. **2014**. Axial vessel widening in arborescent monocots. *Tree Physiology* **34**: 137–145.

R Core Development Team. **2018**. R: A Language and Environment for Statistical Computing.

Renninger HJ, McCulloh KA, Phillips N. **2013**. A comparison of the hydraulic efficiency of a palm species (*Iriartea deltoidea*) with other wood types. *Tree Physiology* **33**: 152–160.

Renninger HJ, Phillips N. **2010a**. Wet- vs . Dry-Season Transpiration in an Amazonian Rain Forest Palm *Iriartea deltoidea*. *Biotropica* **42**: 470–478.

Renninger HJ, Phillips N. **2010b**. Intrinsic and extrinsic hydraulic factors in varying sizes of two Amazonian palm species (*Iriartea deltoidea* and *Mauritia flexuosa*) differing in development and growing environment. *American Journal of Botany* **97**: 1926–1936.

Renninger HJ, Phillips N. **2011**. Hydraulic properties of fronds from palms of varying

height and habitat. *Oecologia* **167**: 925–935.

Renninger HJ, Phillips N, Hodel DR. **2009**. Comparative hydraulic and anatomic properties in palm trees (*Washingtonia robusta*) of varying heights: implications for hydraulic limitation to increased height growth. *Trees* **23**: 911–921.

Rodriguez-Dominguez CM, Carins Murphy MR, Lucani C, Brodribb TJ. 2018. Mapping xylem failure in disparate organs of whole plants reveals extreme resistance in olive roots. *New Phytologist* **218**:1025-1035.

Sherwood S, Fu Q. **2014**. A Drier Future? *Science* **343**: 737–739.

Skelton RP, Brodribb TJ, Choat B. **2017**. Casting light on xylem vulnerability in an herbaceous species reveals a lack of segmentation. *New Phytologist* **214**: 561–569.

Sperling O, Shapira O, Schwartz A, Lazarovitch N. **2015**. Direct in vivo evidence of immense stem water exploitation in irrigated date palms. *Journal of ex* **66**: 333–338.

Sperry JS. **1985**. Xylem embolism in the palm *Rhapis excelsa*. *IAWA Bulletin* **6**: 283–292.

Thomas R, Boura A. **2015**. Palm stem anatomy: phylogenetic or climatic signal? *Botanical Journal of the Linnean Society* **178**: 467–488.

Tomlinson PB. **1990**. *The structural biology of palms*. New York: Oxford University Press.

Tomlinson PB. **2006**. The uniqueness of palms. *Botanical Journal of the Linnean Society* **151**: 5–14.

Tomlinson PB, Fisher JB, Spangler RE, Richer R a. 2001. Stem Vascular Architecture in the Rattan Palm Calamus (Arecaceae – Calamoideae – Calaminae). *American Journal of Botany* **88**: 797–809.

Tomlinson PB, Horn JW, Fisher JB. **2011**. *The anatomy of palms : Arecaceae - Palmae*.

Oxford University Press.

Torres-Ruiz JM, Cochard H, Mayr S, Beikircher B, Diaz-Espejo A, Rodriguez-Dominguez CM, Badel E, Fernández JE. **2014**. Vulnerability to cavitation in *Olea europaea* current-year shoots: further evidence of an open-vessel artifact associated with centrifuge and air-injection techniques. *Physiologia Plantarum* **152**: 465–474.

Torres-Ruiz JM, Cochard H, Choat B, Jansen S, Rosana L, Tomáskova I, Padilla-Díaz CM, Badel E, Burlett R, King A, *et al.* 2017. Xylem resistance to embolism: presenting a simple diagnostic test for the open vessel artefact. *New Phytologist* **215**: 489–499.

Tyree MT, Zimmermann MH. **2002**. *Xylem Structure and the Ascent of Sap*. Berlin, Heidelberg: Springer Berlin Heidelberg.

Urli M, Porté AJ, Cochard H, Guengant Y, Burlett R, Delzon S. **2013**. Xylem embolism threshold for catastrophic hydraulic failure in angiosperm trees. *Tree Physiology* **33**: 672–683.

Zimmermann MH. **1982**. Functional xylem anatomy of angiosperm trees. In: Baas P, ed. New Perspectives in Wood Anatomy. Dordrecht: Springer, 59–70.

Zimmermann MH, Sperry JS. **1983**. Anatomy of the palm *Rhapis excelsa*, IX. Xylem structure of the leaf insertion. *Arnold Arboretum of Harvard University* **64**: 599–609.

Figure legends

Fig. 1. Embolism resistance in palms species occurring in different biomes in comparison with other plants. (a) Embolism resistance of angiosperms and gymnosperm species per biome (Choat *et al.*, 2012). (b) Embolism resistance in palm species per biome. Note that only the six (out of 14) terrestrial biomes where palms can occur are represented here. Biome classification follows Olson (2001). The size of the bars (except for *Trachycarpus fortunei*) represent species P_{50} with their standard error as error bars. Data on *Iriartea deltoidea* from Renninger *et al.* (2011). The asteristic (*) denotes that we could not obtain P_{50} values for this species as little embolism was observed at -8MPa (see results for details).

Fig. 2. Drought-induced xylem embolism resistance for three palm species (*Chamaredorea radicalis*, *Howea, forsteriana* and *Rhapis excelsa*). Vulnerability curves per species obtained by direct observation of petioles of intact palm plants leaves (X-ray micro-computed tomography- micro-CT, dashed lines) and leaflets of detached leaves (optical vulnerability method, continuous). Black points correspond to individual micro-CT sample values, grey shadow bands are 95% confidence interval.

Fig. 3. Frequency distribution vessel area per species and embolism stage.

Fig. 4. Two-dimensional (2D) digital cross-section X-ray microtomography (micro-CT) images of petioles in desiccating intact plants. Species [*Chamaredorea radicalis* (A-C), *Howea, forsteriana* (D-F), *Rhapis excelsa* (G-I) and *Trachycarpus fortunei* (J-L)] are oriented in rows and desiccation stages (all vessels full of sap, onset of embolism and advanced stages of embolism) in columns. Embolized vessels and air spaces are shown in black. Water potential of the plant at the moment of the image is shown in the top-right corner of each image. Insets show a single vascular bundle isolated from the full image (not in scale). Image

sequences show incomparable amounts of petiole shrinkage and parenchyma damage among species. Bars, 500 µm.

Fig. 5. Two-dimensional (2D) digital longitudinal sections X-ray microtomography (micro-CT) images of petioles in desiccating intact plants of *Chamaredorea radicalis, Howea, forsteriana, Rhapis excelsa and Trachycarpus fortunei*. Arrows point to parenchymatic cells (PA), vascular bundles (VB), intercellular spaces air (black) and water filled vessels (dark grey shades). Bars, 100 µm.

Fig. 6. Embolism spread in leaves imaged using a transmission light scanner. Species (*Chamaredorea radicalis, Howea forsteriana* and *Rhapis excelsa*) are oriented in rows and embolism spread stages (onset of embolism, propagation to minor veins and advanced stages of embolism) in columns. Embolism events are coloured in relation to the time of occurrence after the first embolism event, with cooler colours (dark blue/purple) representing earlier events than warmer colours (red/orange/yellow). The first embolism event normally happens in a large parallel vein and then extends to minor parallel and cross veins. A time comparison of embolism propagation can be observed in Supplementary data Movie S12.

TABLES

Table 1. Comparison of vulnerability curves parameters between species and leaf section.

Species	Leaf section	Method	P12	P50	P88	Slope
Chamaedorea radicalis	Blade	Optical vulnerability	-3.12±0.15 ^{A}	-3.3±0.16^{A}	-3.47±0.18 ^{A}	320.05 ^{A}
Howea forsteriana			-3.75±0.29 ^{A}	-4.08±0.38^{A}	-4.41±0.49 ^{A}	213.32 ^{A}
Rhapis excelsa			-5.3±0.18 ^{B}	-5.85±0.13^{B}	-6.4±0.25 ^{B}	151.01 ^{A}
Dypsis baronii	Petiole	Cavitron	-1.17±0.27 ^{a}	-2.24±0.16 a	-3.31±0.12^{a}	50.08 ^{a}
Dypsis decaryi			-1.51±0.23 ^{a}	-2.79±0.12 b	-4.06±0.09 ^{b}	42.09 ^{a}
Dypsis lutescens			-1.58±0.21 ^{a}	-2.59±0.09 ab	-3.6±0.09 ^{ab}	56.29 ^{a}
Chamaedorea radicalis	Petiole	MicroCT	-2.23±0.29 ^{ab}	-2.63±0.1ab	-3.03±0.1^{a}	325.78 ^{a}
Howea forsteriana			-2.9±0.18 ^{b}	-3.14±0.04b	-3.38±0.12^{a}	497.66 ^{a}
Rhapis excelsa			-5.56±0.18^{c}	-5.82±0.2^{c}	-6.09±0.33^{c}	616.51 ^{a}

P_{12}, P_{50}, P_{88} are the xylem potential associated with 12%, 50% and 88% loss of hydraulic conductance, respectively.Values are mean and standard error (SE). Superscript letters for P_{50} represent significative differences between species following the results of statiscal analysis (Tukey's multiple comparisons with 95% family-wise confidence level, Supplementary data Table S4). Note that comparisons were drawn only within the same leaf section and reported in capitals for leaf blade and small caps for petiole comparisons. For results on comparisons between leaf-sections, please check Fig. 4.

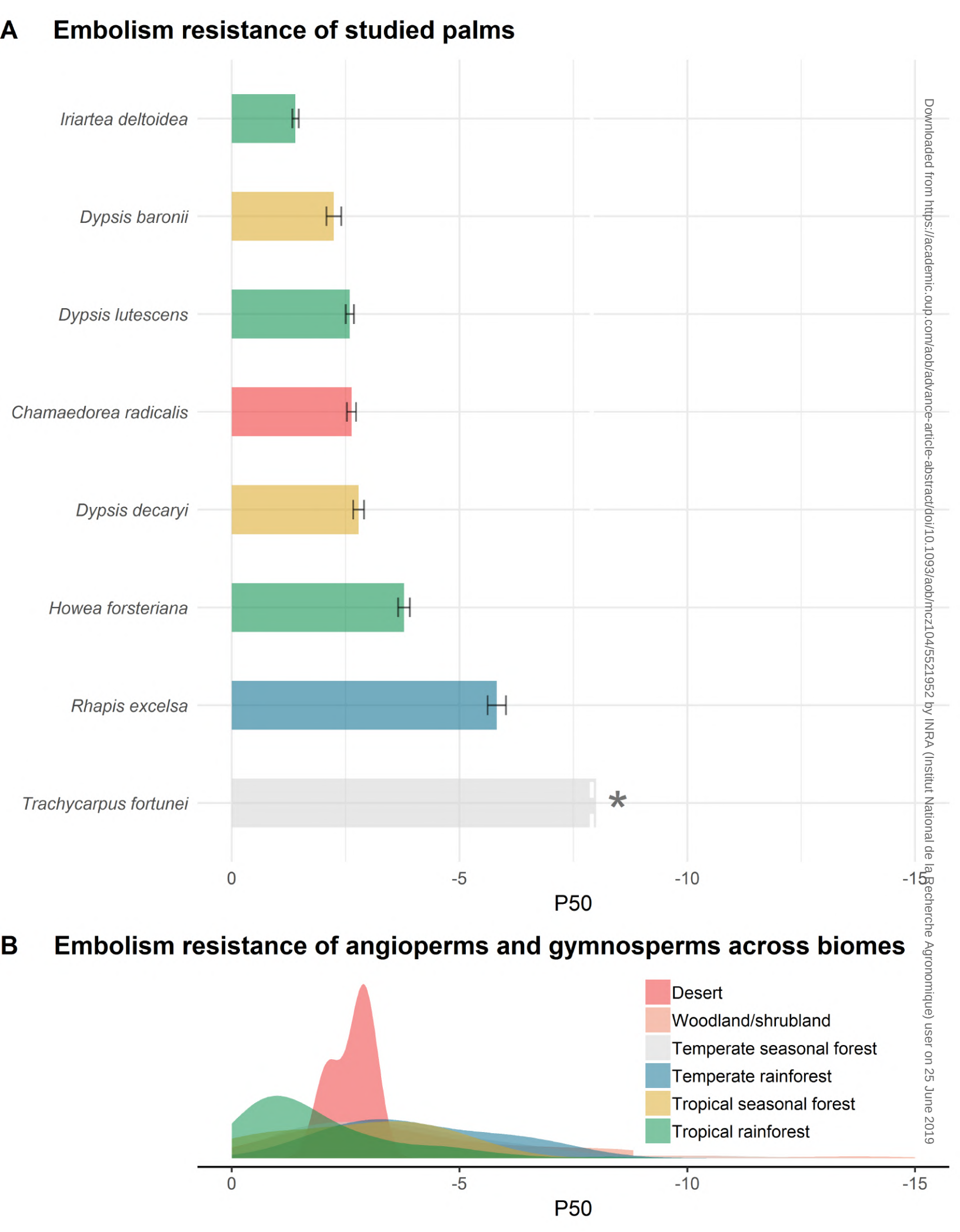

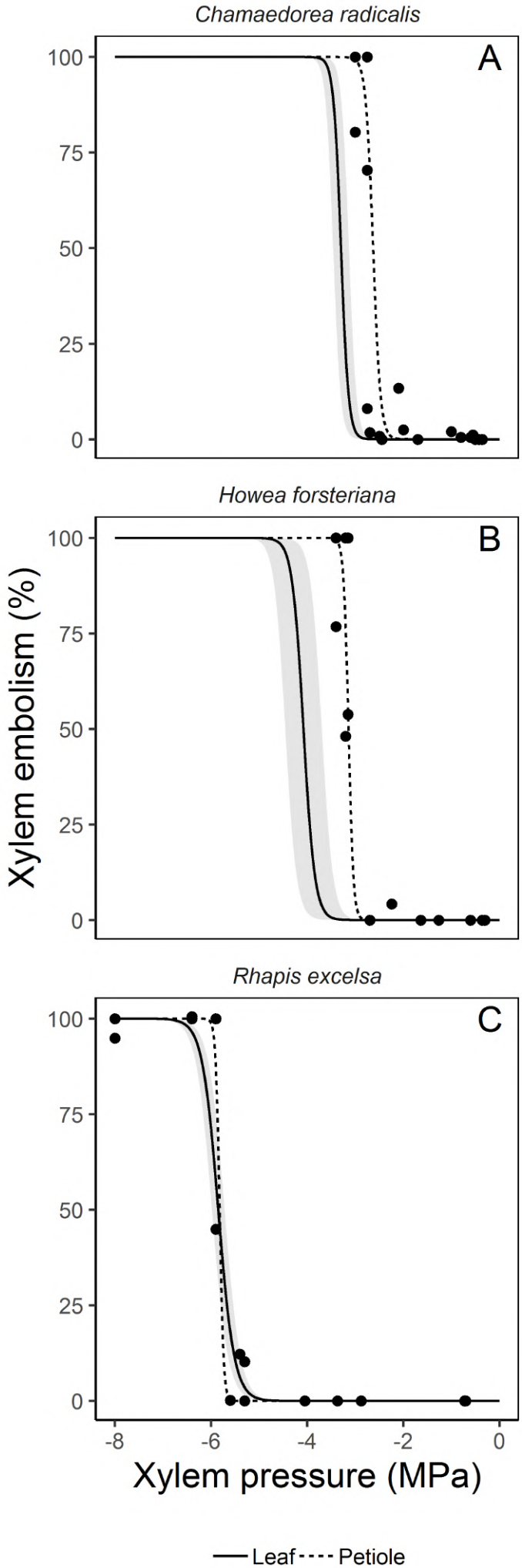

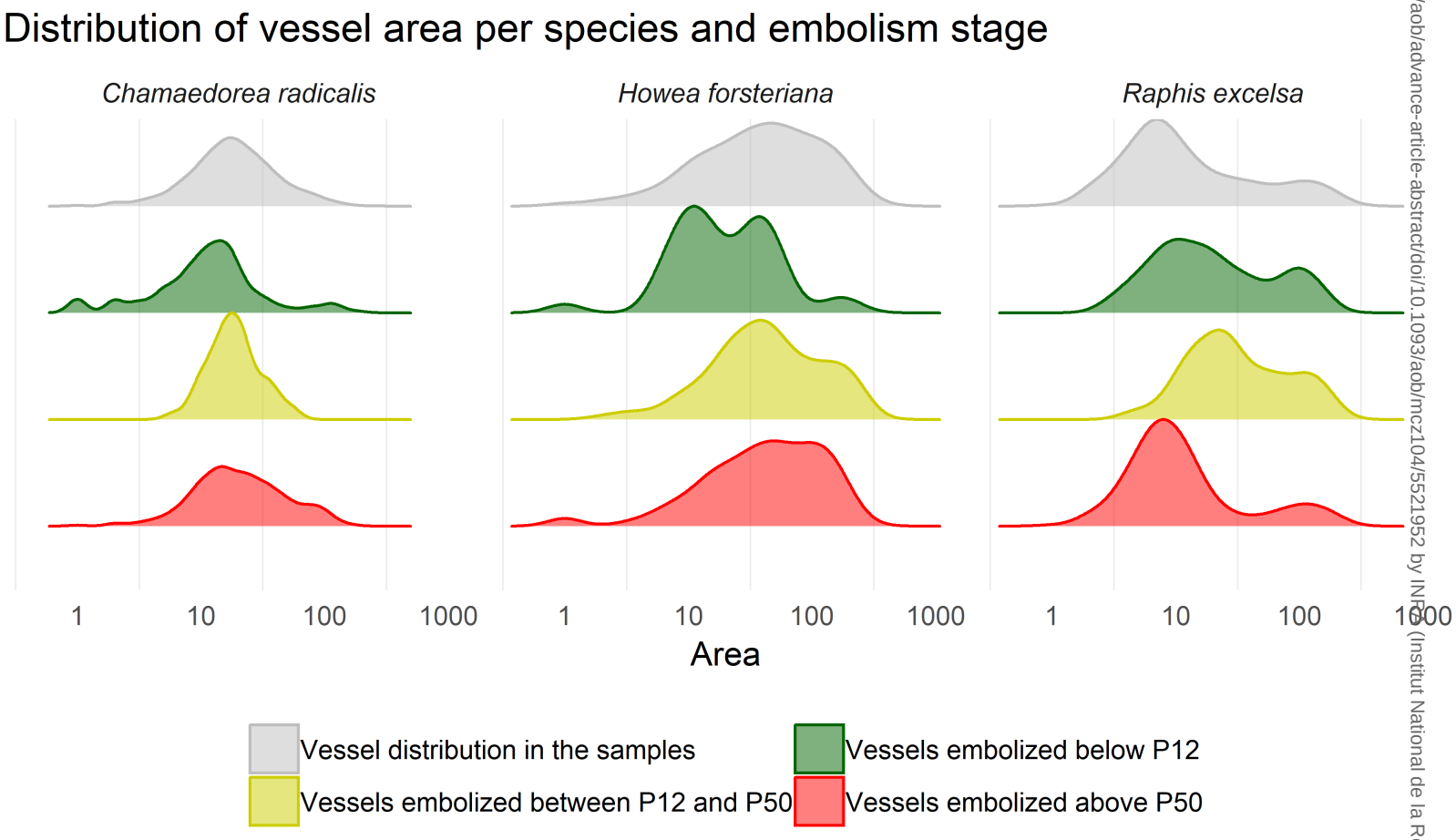

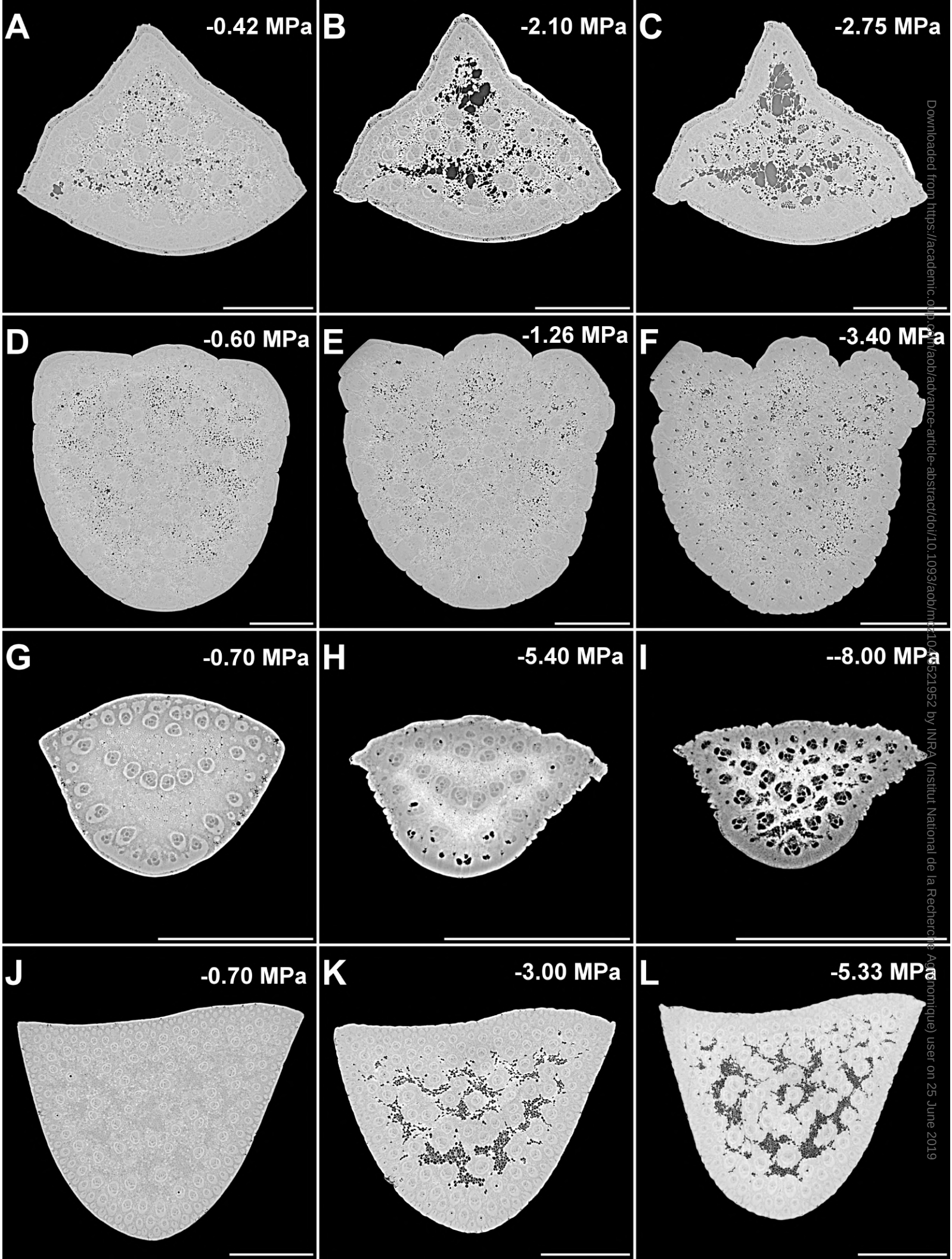

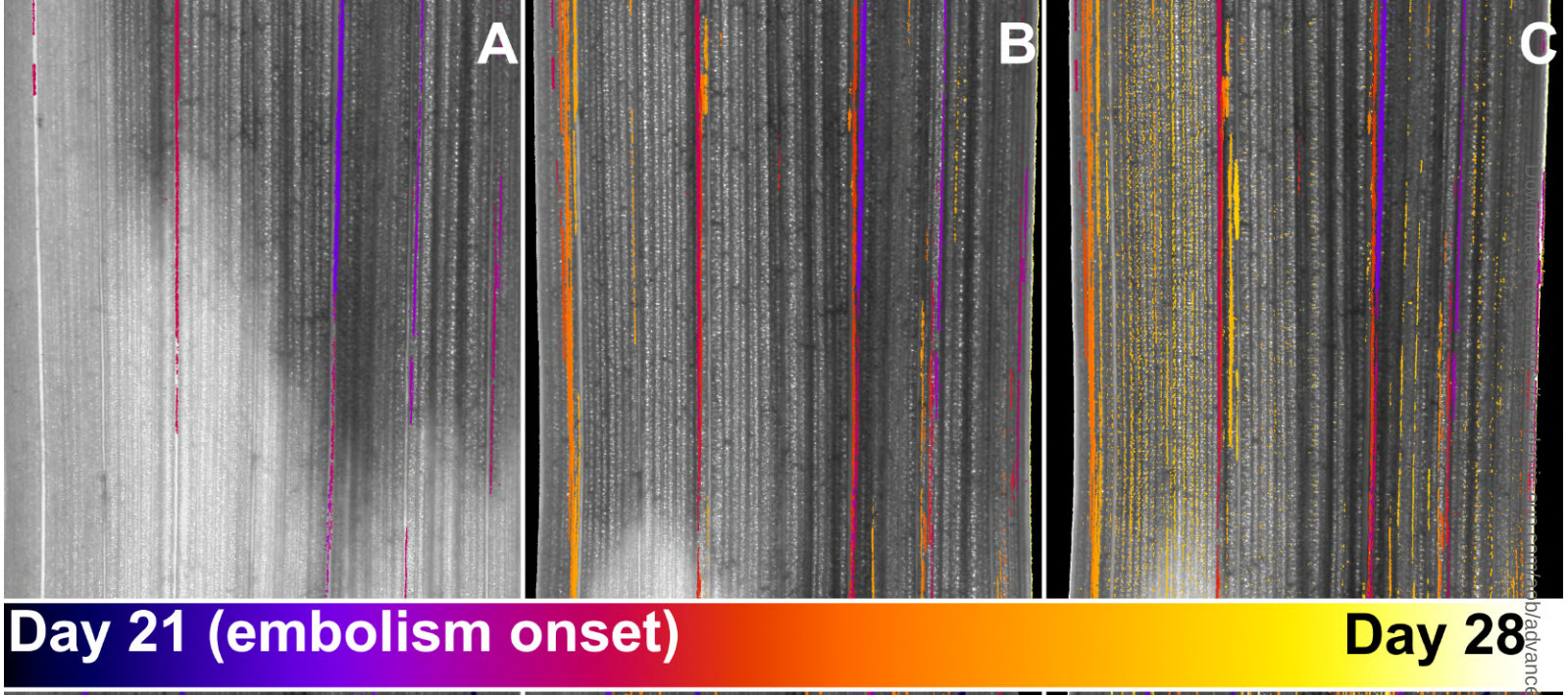
A
B
C
Day 21 (embolism onset)
Day 28

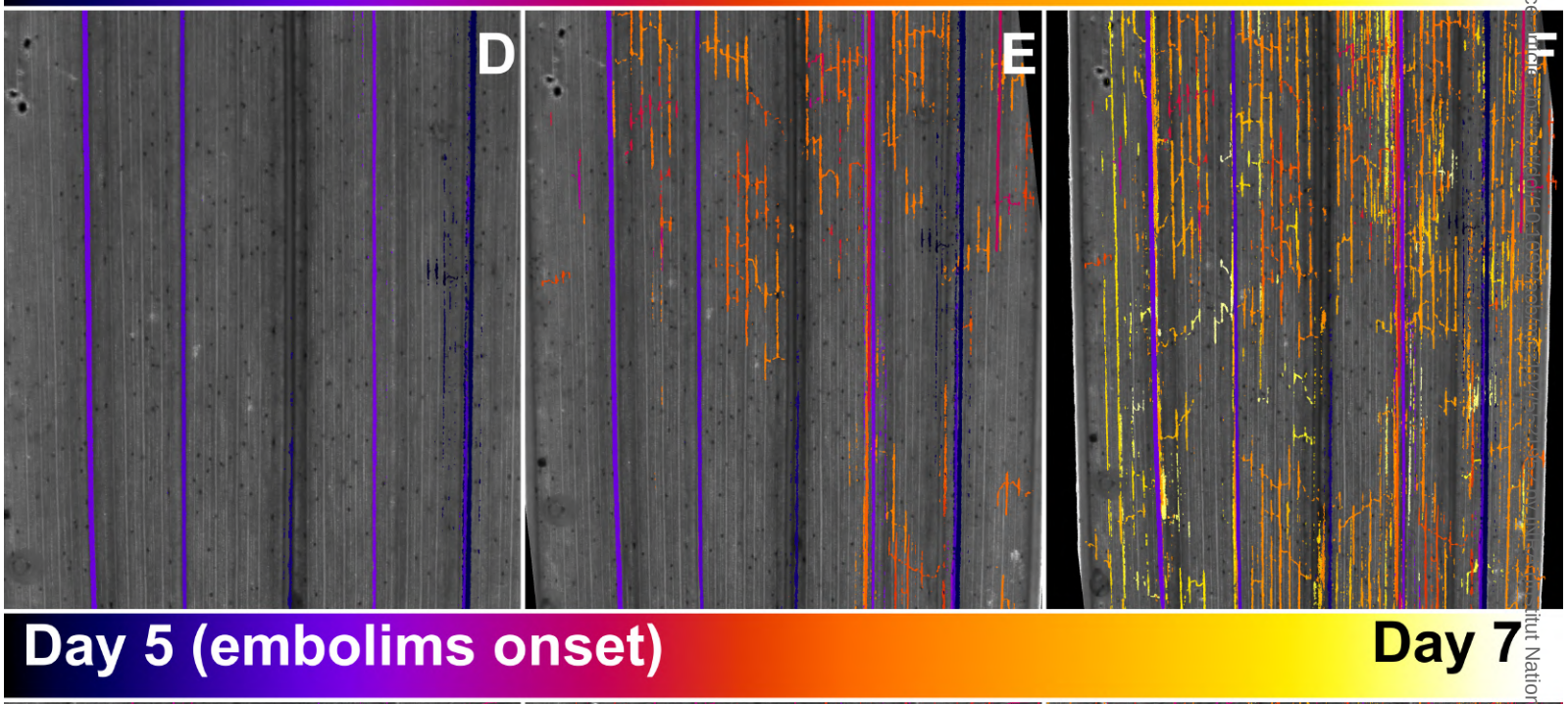
D
E
Day 5 (embolims onset)
Day 7

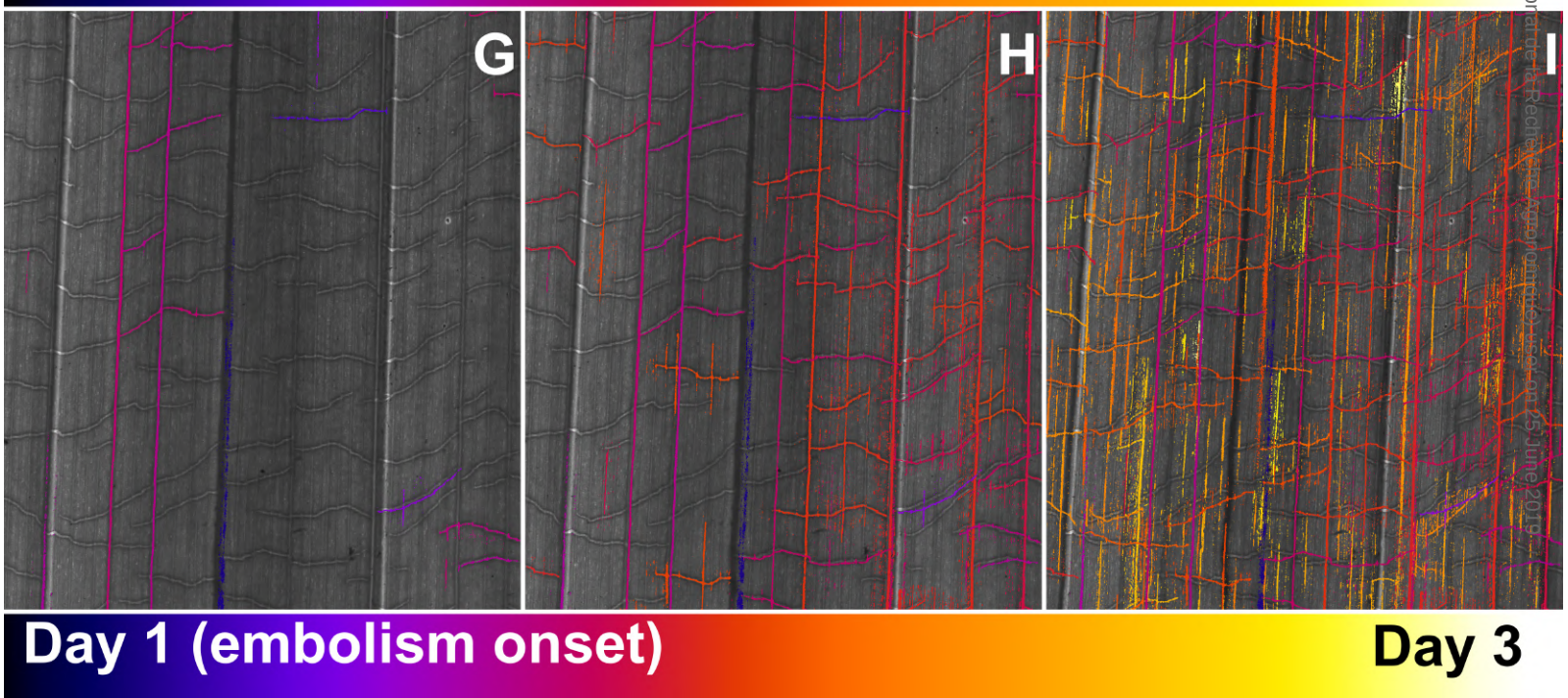
G
H
I
Day 1 (embolism onset)
Day 3